Fibers and Polymers 2015, Vol.16, No.10, 2258-2265
DOI 10.1007/s12221-015-5212-2

ISSN 1229-9197 (print version)
ISSN 1875-0052 (electronic version)

Modeling and Experimental Validation of Transverse Compressive Behavior of Sepiolite Reinforced Rubber Composites

Xiaoming Yu, Boqin Gu*, and Bin Zhang

School of Mechanical and Power Engineering, Nanjing Tech University, Nanjing 211816, China
(Received March 18, 2015; Revised July 15, 2015; Accepted July 20, 2015)

Abstract: This paper presents an experimental and numerical study on the transverse compressive behavior of sepiolite reinforced rubber sealing composites (SRRC). A finite element model of the representative volume element (RVE) extracted from the mesoscopic structure is established, in which the fibers are randomly distributed and the cohesive elements are embedded in the fiber/matrix interface. The RVE model with different sepiolite fiber volume fractions (20 %, 33 % and 42 %) are analyzed, where the interface with perfect bonding condition or not is considered. On the assumption that the fiber/matrix interface is perfect bonded, the compressive stress-strain curve of SRRC with the fiber volume fraction of 33 % is obtained. The result indicates that the assumption of perfect bonding is not appropriate to predict the compressive behavior of SRRC when the compressive strain is larger than 0.1. An interfacial parametric study with the fiber volume fraction of 33 % is carried out to assess the effect of the interfacial properties on the stress-strain relationship. It is found that the simulation results agree well with the experimental result when the interfacial strength is 2 MPa and the interfacial fracture energy is larger than 0.5 J/m^2. The effects of different fiber volume fractions (20 % and 42 %) with the certain interfacial parameters on the compressive behavior of SRRC are investigated. The results reveal that the predictions agree well with experimental data, which indicates that the proposed approach gives an advantage in evaluating the transverse compression behavior of SRRC without further morphological experiments.

Keywords: Micromechanical model, Rubber composites, Sepiolite fiber, Transverse compression, Interfacial debonding

Introduction

Short-fiber-reinforced rubber matrix sealing composites (SRRC) have been used in aerospace and other fields as structural materials for decades owing to their outstanding specific stiffness and strength, and more extensive applications will be found in the future [1,2]. However, till now, there is still no precise approach to predict the strength of these heterogeneous materials, especially in the plane perpendicular to the fibers. Generally, a full experimental approach is used to obtain their strengths, which requires a considerable amount of human, financial and time resources. As compared with the longitudinal properties, the experimental characterization of the transverse properties of SRRC is subjected to more uncertainties and experimental data are actually scarce. Therefore, to establish an accurate and cost-effective method to reveal the damage process of the composites and then to predict their strengths is of great importance.

Over the past 20 years, the polymer/clay composites have shown the benefits for their mechanical properties [3-5], permeability, and fire retardancy. Elastomer/clay composites are an important subgroup of these materials, with one of the most commonly used elastomers being natural rubber. Sepiolite fiber is a kind of porous mineral clay materials widely existing in nature in the form of fiber assemblies [6,7]. The price of the sepiolite fiber is much less than carbon fiber, aramid fiber, and glass fiber. Most mineral sepiolite fiber is produced in China, Spain, Turkey, and the USA. Since Spanish, Turkish, and US sepiolite fibers have bulky or short-fibrous particle shapes, such sepiolites are limits in their potential shapes. On the other hand, Chinese sepiolite fiber has fibrous particles shapes. The shape is a strong advantage for use in composites applicable to structural, heat-insulting and so on [8]. Although the sepiolite fiber as a simple and cheap way to obtain mineral material is available for practical use, it has been less investigated. Therefore, the recent studies on the sepiolite fiber reinforced rubber matrix sealing composites have not fully explored the potential of the sepiolite fiber minerals, which provides promising future for further research.

To guide the practical production and study on the new type of composites, it is necessary to set up the relationship between the mesoscopic structure and macro mechanical properties. The performance of composites such as the fiber reinforced resin matrix, metal matrix, etc., can be accurately predicted by mesoscopic numerical models [9-11]. However, the rubber matrix composites make the mechanical behavior more complicated due to the special performances of rubber (small modulus, large deformation, the hyperelastic, etc.), so that related research is infrequent [12-14].

Computational micromechanics is emerging as an accurate tool to study the mechanical behavior of composites due to the sophistication of the modeling tools and the ever-increasing power of digital computers. Within this framework, the macroscopic properties of a composite can be obtained by means of the numerical simulation of the deformation and failure of a representative volume element (RVE) [15-17]. As compared with the classic homogenization techniques,

*Corresponding author: bqgu@njtech.edu.cn

computational micromechanics present two important advantages. Firstly, the influence of the geometry and spatial distribution of the phases can be accurately taken into account. Kari *et al.* evaluated the effective material properties of randomly distributed short fiber with the changes in volume fraction and aspect ratio of the fiber [18]. Trias *et al.* compared stress and strain distributions between a periodic and a random model for the carbon fiber reinforced polymer composites. The results showed that the periodic models can be used for the simulation of effective properties but random models must be considered for the simulation of local phenomena such as local damage or matrix cracking [19]. In Lee's recent research [20], the fiber length distribution and the fiber orientation in the fiber reinforced composites were concerned, which were regarded as important factors in determining mechanical properties of the composites. Secondly, the details of the stress and strain microfields throughout the microstructure are resolved, which leads to the precise estimation of the onset and propagation of damage, and to accurate prediction of the failure strength. Vaughan *et al.* studied the effect of the fiber-matrix debonding and thermal residual stress on the transverse damage behavior of a unidirectional carbon fiber reinforced epoxy composite. The results showed that the fiber-matrix debonding and matrix plasticity played an important role in forming the macroscopic response of composites [21]. González *et al.* investigated the compressive strength under transverse loading of the fiber reinforced polymers by means of computational micromechanics. The results showed that the role played by the two dominant damage mechanisms (decohesion at the interface and shear band formation in the matrix) in controlling the strength of composites [22]. The previous work illustrates that the spatial random distribution of the sepiolite fiber can be taken into account by the computational micromechanics method. Since the diameter and the length of the sepiolite fiber are only about 0.1 μm and 1 μm, respectively, the interface shear strength of SRRC is very difficult to be measured by the micromechanical test. The computational micromechanics method has become an effective approach instead of the experiment and can also provide a means for analyzing microstructural damage initiation and evolution.

Systematic researches on gasket compressive performances and their characterizations have been carried out in the Fluid Engineering and Sealing Technology Laboratory at Nanjing Tech University [2,23]. This paper presents an extension of the previous work to model the transverse compressive behavior of SRRC with the randomly distributed sepiolite fiber. A finite element model is established, in which the fibers are random distribution and the cohesive elements are embedded in the fiber/matrix interface. The mechanical behavior of SRRC under transverse compression in the plane perpendicular to the sepiolite fiber is investigated numerically and experimentally. The stress-strain relationship is computed by means of the finite element analysis of the representative volume element (RVE) of the composite. The effect of interfacial debonding on the transverse compression behavior of SRRC is investigated. It is obvious that further development and optimization of models would greatly benefit from experimental results to validate the results. The obtained experimental results can be used to estimate the accuracy of simulations for SRRC. Then a parametrical study is carried out to assess the influence of interfacial properties on the stress-strain relationship of SRRC, so as to provide a more clear comprehension about the simulation results.

Expremental

Materials

Acrylonitrile-butadiene rubber (NBR; NBR-3345) is copolymer of acrylonitrile (31-35 %) and butadiene-1.3. NBR-3345 and conventional sulfur curing additive were purchased from Nanjing Rubber Co. Sepiolite fiber was obtained from Hefei Asbestos Co. Other chemicals were purchased from Nanjing Chemical Reagents Co. The component proportions of SRRC are given in Table 1.

Processing

The samples were prepared by a molding process which was similar to that of the traditional rubber based composites [2,24], as shown in Figure 1. The plastication was carried out using a mill mixer (XK160-320) to improve plasticity of raw rubber. Before this step, raw rubber was roasted in a hot chamber within 60-70 °C to decrease its hardness and improve manufacturability. The roll temperature of the mill mixer was controlled below 70 °C, and the roller space was about 0.5-1 mm. The gross rubber was obtained in the mixing step, where all accessory ingredients were dispersed

Table 1. Component proportion of SRRC

Component	Weight content (wt%)
NBR-3345	100
Sepiolite fiber	50, 100, 150
Sulphur	2
ZnO	2.5
Stearic acid	1
Accelerating agent	2
Anti-aging agent	2.5

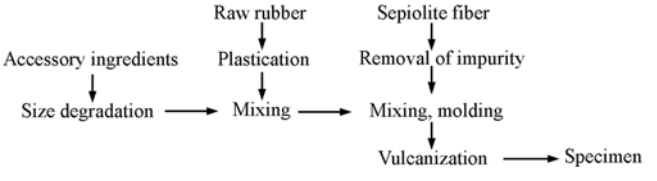

Figure 1. Molding process of SRRC.

evenly in plasticity rubber by repeated extrusion and shearing actions of rollers.

The mixing step was also carried out in a mill mixer. During mixing, the sepiolite fiber was dispersed evenly in gross rubber, and the aspect ratio of the sepiolite fiber was reduced to an appropriate value. The general orientation of the sepiolite fiber was assumed to be in the milling direction, as reported by Senapati and coworkers [25]. The oriented samples were then piled into the compression mold by preservation of the sepiolite fiber orientation and cured at 155 °C for 20 min under the pressure of 16 MPa on a heating press.

Testing

The dumbbell-shaped composite specimens in perpendicular directions with respect to the mill direction were the die cut from the compression molded sheet and the testing was done after 24 h of maturation at room temperature. The compression properties were measured according to ASTM D412-98A with a tensile testing machine (INSTRON 3367). In the analysis process, the mass ratios of the sepiolite fiber to NBR in the specimens are chosen as 0.5:1, 1:1 and 1.5:1. The number of specimens for each sample is three. The test results are obtained by the average value of measurement data.

Computational Micromechanics Model

Generation of the Representative Volume Element

In order to reduce the computational effort, only a representative volume element (RVE) is modeled using periodic boundary conditions. All the sepiolite fibers are aligned in a square RVE of dimensions $L \times L$ and the simulations are focused on the behavior in the plane perpendicular to the sepiolite fibers. A representative of a simple microstructure stands for a more realistic microstructure as shown in Figure 2, which contains a random and homogeneous dispersion of the sepiolite fibers in the matrix. It is assumed that the RVE is periodic and thus the microstructure can be obtained by translating the square RVE along horizontal and vertical directions.

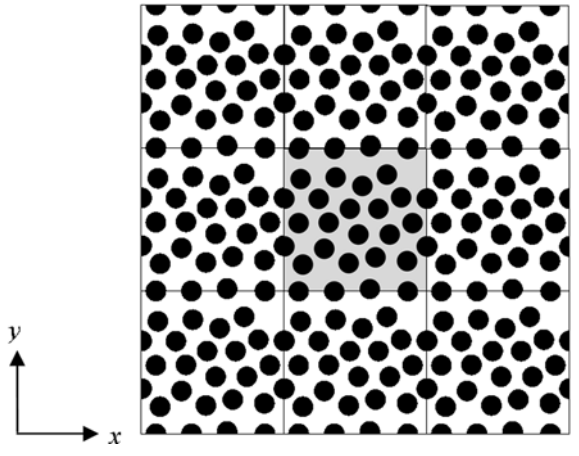

Figure 2. Representation of the microstructure of SRRC with random fiber distribution.

The sepiolite fiber distribution is generated using the random sequential adsorption (RSA) algorithm [26,27], which ensures a random and homogeneous distribution of the sepiolite fiber. The diameter d of the sepiolite fiber is about 0.1 μm. The coordinates of the sepiolite fiber centers are generated randomly and sequentially, and each new sepiolite fiber is accepted if the distance between the neighboring sepiolite fiber surfaces is larger than a minimum value ($0.035d$) to ensure an adequate discretization of this region. In addition, the sepiolite fiber surface should not be too close ($\geq 0.05d$) to the edges and corners of the RVE to avoid the presence of distorted elements during meshing. The sepiolite fibers intersecting the RVE edges are split into an appropriate number of parts and copies to the opposite sides of the square RVE to create a periodic microstructure.

It is important to establish the model of the RVE model with the minimum size to ensure that the predictions of the mechanical behavior obtained by computational micromechanics are close enough to the "exact" solution of the problem in the limiting case $d \ll L$. Rigorous estimates for the critical size of the RVE have been obtained within the framework of linear elasticity, and they show that this size is quite small [28]. The error can be maintained below 5 % if $L/d > 5$ and this ratio of the RVE/reinforcement size will normally lead to errors in the range of 2 % [22,29]. Thus the length (L) of the RVE is about 0.75 μm calculated by the diameter of the sepiolite fiber of 0.1 μm, which is adequate to represent the macroscopic material in our investigation.

Finite Element Model (FEM)

A finite element model is established using ABAQUS/Explicit (2010) code, which uses an explicit direct-integration procedure to overcome the convergence difficulty of numerical analysis. Both the rubber matrix and sepiolite fiber are modeled as elastic continua, using plane strain elements. The RVE is defined with periodic boundary conditions. Both x and y are perpendicular to the direction of the sepiolite fiber and y is aligned with the direction of extension of the specimens tested. The meshing of opposite faces of the RVE is identical, and hence the boundary conditions can be applied directly on the edge nodes using the equation command in ABAQUS. The boundary conditions are expressed mathematically as:

$$\begin{aligned} u_y(x, L) &= -\delta_y \\ u_x(0, y) &= u_x(L, y) = \delta_x \\ u_y(x, 0) &= 0 \end{aligned} \tag{1}$$

where u_x and u_y are the displacements in the x and y

direction, respectively. The above boundary conditions imply that the dimensions of the RVE are allowed to change with respect to the undeformed configuration, but they have to remain uniform within the model.

The Properties of Constituent Material

The sepiolite fiber is modeled as a linearly elastic, homogeneously isotropic material. The Young's modulus and Poisson's ratio of the sepiolite fiber are E_f=86 GPa and v_f=0.2, respectively [30]. The rubber matrix is modeled as a hyperelastic material. The Neo-Hookean model was introduced [31], where W is the strain energy density function. The strain energy density function for an incompressible Neo-Hookean material is as follows:

$$W = C_1(\bar{I}_1 - 3) \tag{2}$$

where C_1 is an empirically determined material constant, and $\bar{I}_1$ is the invariant of the deviatoric component of the left Cauchy-Green deformation tensor.

It is a convenient way to define the material model of hyperelastic composites by means of providing rubber uniaxial test data to ABAQUS. The type of strain potential energy can then be determined according to the contrast diagrams of stress-strain curves given in ABAQUS. A Neo - Hookean model is employed in this paper. The computed parameter C_1 is 1.466 MPa. The sepiolite fibers and matrix are meshed with predominantly 4-node bilinear plane strain quadrilateral, reduced integration elements (CPE4R) with hourglass control and a few 3-node triangle elements (CPE3) [32]. A layer of 4-node two-dimensional cohesive elements COH2D4 is introduced between each the sepiolite fiber and the surrounding matrix to simulate the interfacial debonding. A typical model comprises approximately 50,000 elements and the analyses carried out with finer meshes (up to 80,000 elements) provide the same results.

Cohesive Zone Model

The cohesive zone model is employed to describe the damage of interface. The mechanical behavior of these elements is expressed in terms of a traction-separation law which relates the displacement jump across the interface with the traction vector acting upon it. An element size of nearly $0.03r_f$, where r_f is the sepiolite fiber radius, is used in a vicinity of the interface [33]. The initial response is linear in absence of damage and, therefore, the traction-separation law can be written as:

$$t_n = K\delta_n \text{ and } t_s = K\delta_s \tag{3}$$

where t_n, t_s, δ_n and δ_s stand for the normal and tangential tractions and displacement jumps across the interface respectively. The initial response is linear in absence of damage with an elastic stiffness of K. An elastic stiffness K= 10^8 GPa/m is selected for the interface, which is large enough to ensure the displacement continuity at the interface and to avoid any modification of the stress field around the fibers in the absence of damage [22].

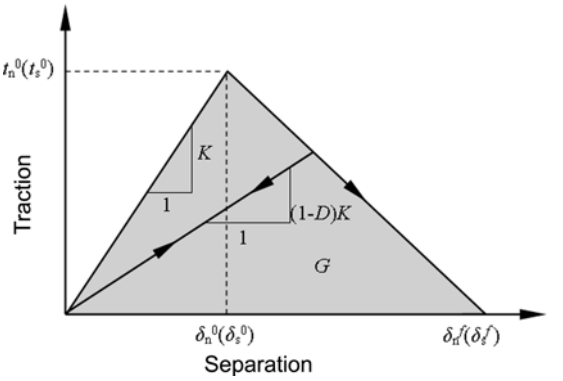

Figure 3. Traction-separation law of the cohesive element.

Damage is assumed to be initiated when the maximum nominal stress ratio reaches one of the values given by following equation:

$$\max\left\{\frac{<t_n>}{t_n^0}, \frac{t_s}{t_s^0}\right\} = 1 \tag{4}$$

where <> are the Macaulay brackets, which return the argument if positive and zero otherwise, to impede the development of damage when the interface is under compression, and t_n^0 and t_s^0 are the normal and shear interfacial strengths which were assumed to be equal for simplicity (t_n^0=t_s^0). Once the damage begins, the traction stress is reduced depending on the interface damage parameter D, which evolves from 0 (in the absence of damage) to 1 (at ultimate failure), as shown in Figure 3. The displacement at failure (δ_n^f or δ_s^f) is determined by the fracture energy G, which corresponds to the area under the traction-separation curve.

Results and Discussion

Perfect Bonding

In this paper, the concept of the perfect bonding is defined from the view of damage behavior of composites. That is, bonding in the fiber/matrix interface is fine, so that no interfacial damage occurs between the sepiolite fiber and matrix interfaces. In order to verify the applicability of the assumption of the perfect bonding in the fiber/matrix interface to the stress analysis of SRRC, the compressive stress- strain curve of SRRC with the random sepiolite fiber distribution were investigated by means of both the numerical simulation and the experiment. In the analysis process, the mass ratio of the sepiolite fiber to NBR in the specimens is chosen as 1:1. Since the densities of the sepiolite fiber and NBR are around 2.1 and 1.0 g/cm^3, respectively [34], the

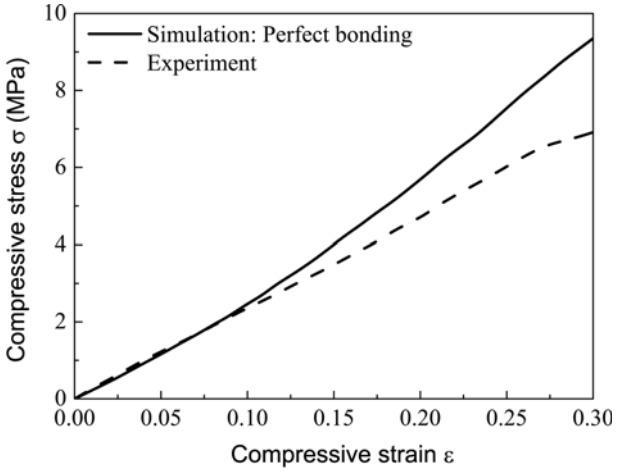

Figure 4. Stress-strain curves with the sepiolite fiber volume fraction of 33 % by the experiment and simulation.

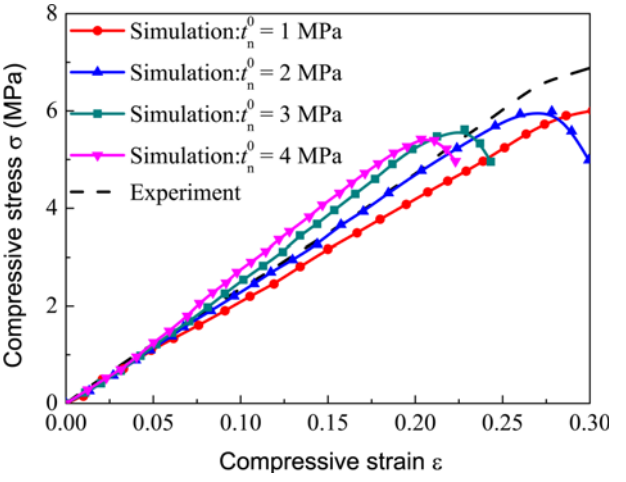

Figure 5. Effect of the interfacial strength on the stress-strain curve under transverse compression.

corresponding sepiolite fiber volume fraction in SRRC is 33 %.

The simulation result from the random RVE is compared to the experimental result, as shown in Figure 4. The simulation result is consistent with experimental result at low strain (less than 0.1). However, there is a large difference as the compressive strain increases. It can be seen that the compressive stress error between the simulation and experimental results is high up to 35 % when the strain reaches to 0.3. The reason is that there are high stress regions at the fiber/matrix interface when the compressive strain reaches to 0.1. The interfacial debonding will happen at these high stress regions, and the performance of SRRC will decrease. Therefore, the experimental result is less than the numerical result when the perfect interfacial bonding is considered.

Debonding Allowed

So far a perfect bonding interface is considered. But interfacial debonding will occur as the compressive strain increases. In the following, an interfacial parametric study with the fiber volume fraction of 33 % is carried out to assess the effect of the interfacial properties on the stress-strain relationship of SRRC.

Effect of Interfacial Strength

The effect of fiber-matrix debonding on the transverse failure behavior is examined using a cohesive element zone model at the fiber-matrix interface. The interfacial strength t_n^0 is used to predict failure behavior of SRRC. Damage evolution at the interface is controlled by the interfacial fracture energy G. For the present analysis, it will be initially assumed that the interfacial fracture energy G is 0.1 J/m^2 [35] and the interfacial strength t_n^0 are from 1 MPa to 4 MPa. According to Chinese national standard GB/T 9129-2003 for the rubber gasket, the compressive stress is set as 7 MPa and

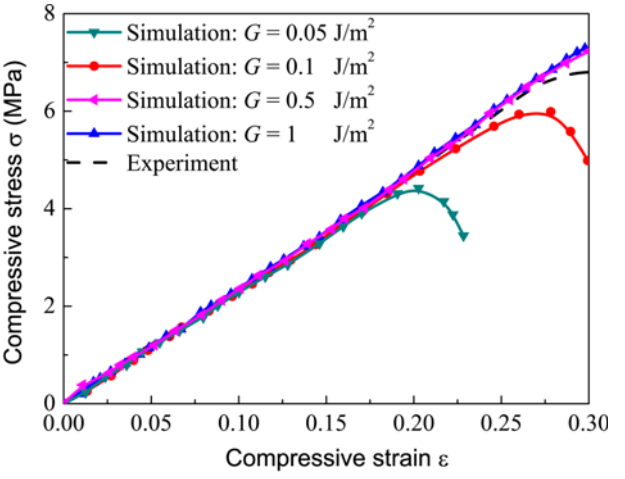

Figure 6. Influence of the interface fracture energy on the stress-strain curve under transverse compression.

the corresponding compressive strain is 0.25±0.1 [2]. It can be seen that the experimental results of SRRC meet this standard. Figure 5 shows that the low interfacial strength corresponds to the small compressive modulus and low strength of composites. It is obvious that the interfacial strength has a significant effect on the macroscopic response of SRRC, with a higher transverse strength being seen for the increasing fiber/matrix interfacial strength. The simulation result with the interfacial strength t_n^0 of 2 MPa is close to the experimental result at low strain. However, there exists a strain softening in the simulation result at the strain of 0.25. The reason is that the chosen interfacial fracture energy G of 0.1 J/m is lower than that of the specimen material, which causes the earlier generation of strain softening.

Effect of Interface Fracture Energy

The effect of interfacial fracture energy on the compressive

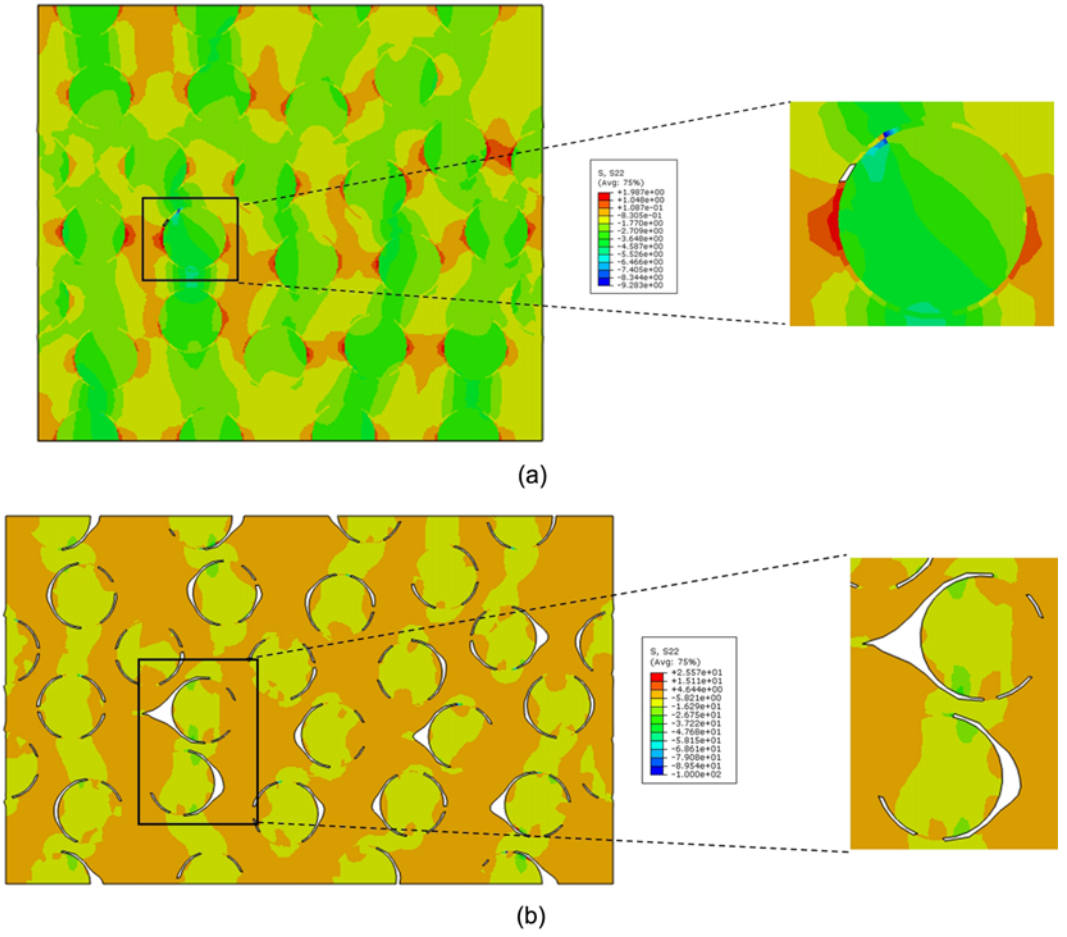

Figure 7. The initiation and evolution of the interfacial debonding with the fiber volume fraction of 33 % (a) ε=0.08 and (b) ε=0.3.

stress-strain curve of SRRC is also examined. Five kinds of the interfacial fracture energies G are considered, which are 0.05, 0.1, 0.5, and 1 J/m^2. Figure 6 shows the transverse response of SRRC which has an interfacial strength t_n^0 of 2 MPa for a range of the interfacial fracture energies. The results indicate that the compressive strength increases with the increase of the interfacial fracture energy. The stress-strain curves of SRRC have a good agreement with experimental result when the interfacial fracture energy $G \geq 0.5$ J/m^2. It can be also found that the stress-strain curves of SRRC remain unchanged when $G \geq 0.5$ J/m^2.

Microscopic Stress State

The compressive stress distribution under transverse loading are studied in SRRC with the sepiolite fiber volume fraction of 33 %. The micromechanical model with the interfacial fracture energy of 0.5 J/m^2 and the interfacial strength of 2 MPa are adopted. The compressive stress distribution along the compressive direction in SRRC is shown in Figure 7. Figure 7(a) shows that the onset of damage occurs at two closely neighboring sepiolite fibers, when the compressive strain is about 0.08. It confirms the reason of the difference between experimental data and simulation results when the perfect bonding interface is assumed. Figure 7(b) shows that the evolution of the interfacial debonding leads to the formation of the interfacial voids when the compressive strain is about 0.3. It can be seen that the interfacial debonding spreads widely throughout the RVE.

Validation of Determined Interfacial Parameters

In order to verify the application of the interfacial parameters to the stress analysis of SRRC, the compressive stress-strain curves of SRRC are investigated both by the numerical simulation and experiment. In the analysis process, the mass ratios of the sepiolite fiber to rubber in the specimens are 0.5:1 and 1.5:1, so the corresponding fiber volume fraction of SRRC is 20 % and 42 %. Figure 8 illustrates the contrast results between experiment and numerical simulation, where the interfacial fracture energy and the interfacial strength are 0.5 J/m^2 and 2 MPa, respectively. The results show that the compressive stress increases as the increase of the sepiolite

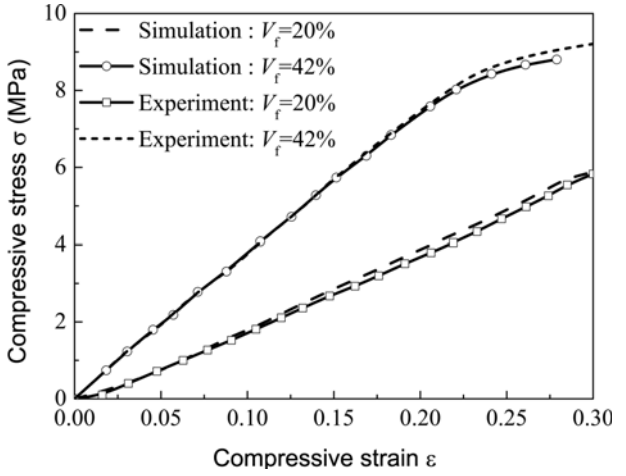

Figure 8. Stress-strain curves with different sepiolite fiber volume fractions by experiments and simulations.

fiber volume fraction at the same compressive strain. The numerical simulation results are in good agreement with the experimental data. Micromechanical modeling with the determined interfacial parameters enables to accurately estimate the behavior of SRRC with different sepiolite fiber volume fractions under the transverse compression.

Conclusion

The samples of sepiolite reinforced rubber composites (SRRC) with three sepiolite fiber volume fractions (20 %, 33 % and 42 %) were prepared and tested. The compressive stress-strain curves of SRRC were obtained.

A finite element model based on representative volume element was established to investigate the transverse compressive behavior of SRRC. In the first set of simulation, the perfect bonding between the sepiolite fibers and the matrix was assumed and the sepiolite fiber volume fraction was 33 %. The results showed that the assumption of perfect bonding was not appropriate to predict the compressive behavior of SRRC when the compressive strain was larger than 0.1. In the second set of simulation, the interfacial debonding between the sepiolite fibers and the matrix was considered by introducing the cohesive elements. It was found that the simulation results had a good agreement with experimental results when the interfacial strength was 2 MPa and interfacial fracture energy was larger than 0.5 J/m^2.

The initiation and evolution of the interfacial debonding with the certain interfacial parameters were analyzed by the numerical simulation. The results showed that the onset of damage occurred at two closely neighboring sepiolite fibers when the compressive strain reaches to about 0.08. The interfacial debonding propagated widely throughout the SRRC and led to the formation of the interfacial voids when the compressive strain was about 0.3.

In order to verify the application of the interfacial parameters, the effects of different sepiolite fiber volume fractions (20 % and 42 %) on the compressive behavior of SRRC were investigated. It was found that the predicted results agreed well with that measured by experiments when the interfacial strength was 2 MPa and interfacial fracture energy was 0.5 J/m^2.

In general, the micromechanical modeling with the determined interfacial parameters in the random RVE enables to accurately estimate the transverse compressive behavior of SRRC with different sepiolite fiber volume fractions. This approach can give an advantage in evaluating the transverse compressive behavior of SRRC without further morphological experiments. To meet the performance requirements of Chinese national standard for the rubber gasket, the interfacial strength of 2 MPa and the interfacial fracture energy larger than 0.5 J/m^2 are necessary.

Acknowledgements

This project is supported by National Natural Science Foundation of China (Grant No. 51375223) and by Jiangsu Province Ordinary University Graduate Research and Innovation Foundation (Grant No. KYZZ15_0230).

References

1. B. Q. Gu, Y. Chen, and J. F. Zhou in "Advances in Composite Materials - Ecodesign and Analysis", 1st ed., pp.21-54, InTech, Rijeka, Croatia, 2011.
2. B. Q. Gu and Y. Chen, *Key Eng. Mater.*, **353**, 1243 (2007).
3. J. H. Lee and Y. G. Jeong, *Fiber. Polym.*, **12**, 180 (2011).
4. M. Joshi, M. Shaw, and B. S. Butola, *Fiber. Polym.*, **5**, 59 (2004).
5. M. Andideh, G. Naderi, M. H. R. Ghoreishy, and S. Soltani, *Fiber. Polym.*, **15**, 814 (2014).
6. C. Chen, J. Liang, F. Wang, Q. Tang, and Y. Chen, *J. Nanosci. Nanotechnol.*, **14**, 3515 (2014).
7. V. H. Orozco, A. F. Vargas, W. Brostow, T. Datashvili, B. L. López, K. Mei, and L. Su, *J. Nanosci. Nanotechnol.*, **14**, 4918 (2014).
8. F. M. Fernandes, A. I. Ruiz, M. Darder, P. Aranda, and E. Ruiz-Hitzky, *J. Nanosci. Nanotechnol.*, **9**, 221 (2009).
9. P. Cui, X. Wang, and X. W. Tangpong, *J. Nanosci. Nanotechnol.*, **12**, 8330 (2012).
10. S. Rana, R. Alagirusamy, and M. Joshi, *J. Nanosci. Nanotechnol.*, **11**, 7033 (2011).
11. H. Zhang, L. Tang, G. Liu, D. Zhang, L. Zhou, and Z. Zhang, *J. Nanosci. Nanotechnol.*, **10**, 7526 (2010).
12. J. Moraleda, J. Segurado, and J. LLorca, *J. Mech. Phys. Solids.*, **57**, 1596 (2009).
13. S. Soltani, G. Naderi, and S. Mohseniyan, *Fiber. Polym.*, **15**, 2360 (2014).
14. X. Li, Y. Xia, Z. Li, and Y. Xia, *Compos. Mater. Sci.*, **55**,

157 (2012).
15. X. Wang, B. Zhang, S. Du, Y. Wu, and X. Sun, *Mater. Des*., **31**, 2464 (2010).
16. J. Xiaoyu, G. Qing, and K. Guozheng, *Compos. Sci. Technol*., **58**, 1685 (1998).
17. H. Huang and R. Talreja, *Compos. Sci. Technol*., **66**, 2743 (2006).
18. S. Kari, H. Berger, and U. Gabbert, *Compos. Mater. Sci*., **39**, 198 (2007).
19. D. Trias, J. Costa, J. A. Mayugo, and J. E. Hurtado, *Compos. Mater. Sci*., **38**, 316 (2006).
20. D. J. Lee, H. Oh, Y. S. Song, and J. R. Youn, *Compos. Sci. Technol*., **72**, 278 (2012).
21. T. J. Vaughan and C. T. McCarthy, *Compos. Sci. Technol*., **71**, 388 (2011).
22. C. González and J. Lorca, *Compos. Sci. Technol*., **67**, 2795 (2007).
23. B. Zhang, B. Gu, and X. Yu, *J. Appl. Polym. Sci*., 132, doi:10.1002/app.41672 (2015).
24. M. Tian, L. Su, W. Cai, S. Yin, and Q. Chen, *J. Appl. Polym. Sci*., **120**, 1439 (2011).
25. C. Hintze, R. Boldt, S. Wiessner, and G. Heinrich, *J. Appl. Polym. Sci*., **130**, 1682 (2013).
26. F. Naddeo, N. Cappetti, and A. Naddeo, *Compos. Mater. Sci*., **81**, 239 (2014).
27. F. Ballani, D. J. Daley, and D. Stoyan, *Compos. Mater. Sci*., **35**, 399 (2006).
28. I. Monetto and W. J. Drugan, *J. Mech. Phys. Solids*, **52**, 359 (2004).
29. J. Segurado and J. Lorca, *Acta Mater*., **53**, 4931 (2005).
30. D. P. N. Vlasveld, M. De Jong, H. E. N. Bersee, A. D. Gotsis, and S. J. Picken, *Polymer*, **46**, 10279 (2005).
31. F. López Jiménez and S. Pellegrino, *Int. J. Solids Struct*., **49**, 635 (2012).
32. L. Yang, Y. Yan, Y. Liu, and Z. Ran, *Compos. Sci. Technol*., **72**, 1818 (2012).
33. M. Romanowicz, *Compos. Mater. Sci*., **47**, 225 (2009).
34. T. Takei, R. Oda, A. Miura, N. Kumada, N. Kinomura, R. Ohki, and H. Koshiyama, *Compos. Pt. B-Eng*., **44**, 260 (2013).
35. J. Moraleda, J. Segurado, and J. Llorca, *Int. J. Solids Struct*., **46**, 4287 (2009).